is equipped with four skewed reaction wheels. The torque distribution matrix from the reaction wheel torque vector $\boldsymbol{\tau}$ to the spacecraft control input vector $\mathbf{u}$ is given as

$$\mathbf{A} = \begin{bmatrix} \cos\beta & -\cos\beta & \cos\beta & -\cos\beta \\ \sin\beta & 0 & -\sin\beta & 0 \\ 0 & -\sin\beta & 0 & \sin\beta \end{bmatrix}$$

where the skew angle β is chosen as 45 deg. The maximum torque level of each reaction wheel is given as $\bar{\tau}_i = 0.3$ N·m, and the maximum slew rate is given as $\dot{\theta}_{\max} = 0.2$ deg/s, which is about 90% of the low-rate gyro measurement capability.

The initial quaternions for a specific reorientation maneuver are given as

$$\hat{\mathbf{q}}(0) = (0.2652,\ 0.2652,\ -0.6930,\ 0.6157)$$

which corresponds to a 104-deg slew angle about the eigenaxis $\mathbf{q}(0) = (0.2652,\ 0.2652,\ -0.6930)$. The slew should ideally be completed in 8.7 min.

(a) Synthesize a saturation control logic of the form

$$\mathbf{u}_c = -\mathbf{K}\,\text{sat}(\mathbf{Pq}) - \mathbf{C}\boldsymbol{\omega}$$

$$\boldsymbol{\tau}_c = \mathbf{A}^{+}\mathbf{u}_c \qquad \text{where } \mathbf{A}^{+} = \mathbf{A}^{T}(\mathbf{A}\mathbf{A}^{T})^{-1}$$

$$\boldsymbol{\tau} = \underset{\sigma}{\text{sat}}(\boldsymbol{\tau}_c)$$

$$\mathbf{u} = \mathbf{A}\boldsymbol{\tau}$$

Hint: If we choose $\zeta = 0.707$ and $\omega_n = 0.1$ rad/s, then we have

$$\mathbf{C} = \text{diag}(889,\ 774,\ 380)$$

$$\mathbf{KP} = \text{diag}(126,\ 110,\ 54)$$

$$\mathbf{K} = \text{diag}(k_1, k_2, k_3)\mathbf{J} = \text{diag}(1.0452, 0.9098, 1.1667)$$

$$\mathbf{P} = k\mathbf{K}^{-1}\mathbf{J} = \text{diag}(120, 120, 46)$$

(b) Perform computer simulation of the closed-loop system, and verify that a near bang-off-bang, eigenaxis maneuver is, in fact, achieved under the slew rate and control torque constraints.

Note: See Ref. 17 for additional information pertaining to this problem.

7.4 Attitude Control and Momentum Management

This section, based on Refs. 18–20, is concerned with the attitude control and momentum management problem of a large space vehicle in low Earth orbit, such as the International Space Station, as shown in Fig. 7.4.

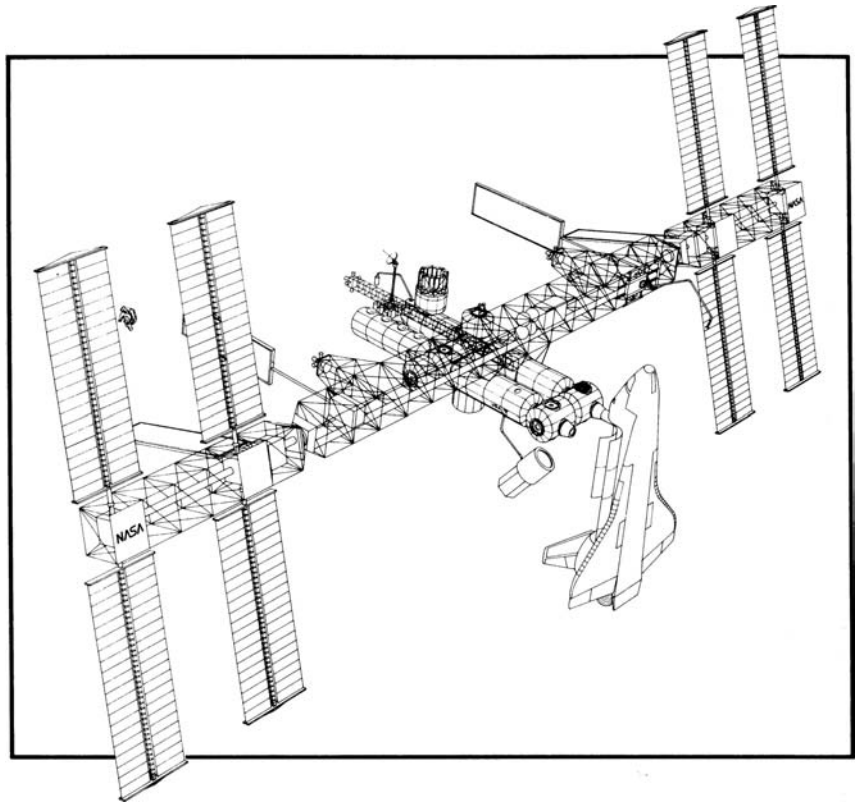

Fig. 7.4 Large space vehicle in low Earth orbit.

7.4.1 Introduction

Large space vehicles, such as Skylab of the 1970s, the Mir space station, and the International Space Station, employ control moment gyros (CMGs) as primary actuating devices during normal flight mode operation. Because the CMGs are momentum exchange devices, external control torques must be used to desaturate the CMGs, that is, bring the momentum back to its nominal value. Some methods for unloading CMG momentum include the use of magnetic torques, reaction jets, and gravity-gradient torque. For a large spacecraft in low Earth orbit, such as the International Space Station, the gravity-gradient torque approach is preferred because it requires no consumables or additional hardware. One approach to CMG momentum management is to integrate the momentum management and attitude control design. In this continuous, closed-loop control of both the CMG momentum and vehicle attitude, the design objective is to establish a proper tradeoff between spacecraft pointing and CMG momentum management, while satisfying the specific mission requirements.

É tratado um exemplo com o atuador CMG. Mas, da forma como as equações são desenvolvidas, o método aplica-se facilmente a rodas de reação, com mudanças mínimas.

O exemplo da ISS é tratado para contextualização. No entanto, o método se aplica a outros veículos espaciais. Inclusive, não vale somente para "grandes" veículos. O termo "grande" é adotado porque CMGs são usados principalmente neste tipo de veículo, ficando as rodas de reação para os menores.

The International Space Station will be controlled by four parallel mounted double-gimbal CMGs. A CMG of the International Space Station consists of a large wheel rotating at a constant speed (6600 rpm) and producing an angular momentum of 3500 ft-lb-s about its spin axis. This rotating wheel is mounted in a two-degree-of-freedom gimbal system that can point the spin axis (momentum vector) of the wheel in any direction, i.e., the tip of the angular momentum vector can be placed anywhere on a sphere of radius 3500 ft-lb-s. The CMG generates an output reaction torque that is applied to the Space Station by inertially changing the direction of its wheel momentum (spin axis). The CMG output torque has two components, one proportional to the rate of change of the CMG gimbals and a second proportional to the inertial body rate of the Space Station as sensed at the CMG base. Because the momentum along the direction of the spin axis is fixed (constant wheel speed), the output torque is constrained to lie in the plane of the wheel. As a result, one CMG is insufficient to provide the three-axis torque needed to control the attitude of the Space Station. To provide attitude control at least two CMGs are required.

The Space Station CMG assembly consists of four parallel mounted double-gimbal CMGs with two of the four CMGs mounted antiparallel with the other two. The four CMGs have a spherical momentum storage capability of 14,000 ft-lb-s, the scalar sum of the individual CMG wheel momentum. The momentum stored in the CMG system at any given time equals the vector sum of the individual CMG momentum vectors. To maintain the desired attitude, the CMG system must cancel, or absorb, the momentum generated by the disturbance torques acting on the Space Station. If the average disturbance torque is nonzero, the resulting CMG output torque will also be nonzero and momentum will build up in the CMG system. Once the CMG system saturates, i.e., all of the CMGs' momentum vectors have become parallel and controllability about the parallel line is lost, it is unable to generate the torque required to cancel the disturbance torque and loss of attitude control results. To prevent the CMG system from saturating, a continuous gravity-gradient momentum management system will be employed for the Space Station.

In this section the CMGs are assumed as ideal torquers, i.e., the CMG gimbal dynamics and CMG steering logic are ignored. The attitude control and momentum management technique to be presented in this section is, however, applicable to any CMG-equipped spacecraft. A brief overview of the CMG steering logic design problem associated with different CMG configurations will be presented later in Sec. 7.5.

Most large spacecraft are, in fact, flexible multibody vehicles with time-varying inertias, as can be seen in Fig. 7.4; however, they can be considered single rigid bodies for the practical design of a low-bandwidth, integrated attitude/momentum controller. All states of the rigid vehicle are usually available for feedback control from the strapdown inertial reference system of the vehicle.

7.4.2 Mathematical Models for Control Design

Consider a rigid spacecraft in low-Earth circular orbit, which is expected to maintain local-vertical and local-horizontal (LVLH) orientation during normal mode operation. As discussed in the preceding chapter, the nonlinear equations

of motion of a rigid body in circular orbit can be written, in terms of components along the body-fixed control axes, as follows.

Attitude kinematics for the $\mathbf{C}_1(\theta_1) \leftarrow \mathbf{C}_3(\theta_3) \leftarrow \mathbf{C}_2(\theta_2)$ sequence:

A adoção da sequência 231 ficou estranha, pois os ângulos de rolamento, arfagem e guinada são usualmente definidos para a sequência 321. Inclusive o modelo desenvolvido nas aulas 7 e 9 (a partir do próprio livro, trata da sequência 321.

$$\begin{bmatrix} \dot{\theta}_1 \\ \dot{\theta}_2 \\ \dot{\theta}_3 \end{bmatrix} = \frac{1}{\cos\theta_3} \begin{bmatrix} \cos\theta_3 & -\cos\theta_1 \sin\theta_3 & \sin\theta_1 \sin\theta_3 \\ 0 & \cos\theta_1 & -\sin\theta_1 \\ 0 & \sin\theta_1 \cos\theta_3 & \cos\theta_1 \cos\theta_3 \end{bmatrix} \begin{bmatrix} \omega_1 \\ \omega_2 \\ \omega_3 \end{bmatrix} + \begin{bmatrix} 0 \\ n \\ 0 \end{bmatrix} \tag{7.111}$$

Rigid-body dynamics:

$$\begin{bmatrix} J_{11} & J_{12} & J_{13} \\ J_{21} & J_{22} & J_{23} \\ J_{31} & J_{32} & J_{33} \end{bmatrix} \begin{bmatrix} \dot{\omega}_1 \\ \dot{\omega}_2 \\ \dot{\omega}_3 \end{bmatrix} = - \begin{bmatrix} 0 & -\omega_3 & \omega_2 \\ \omega_3 & 0 & -\omega_1 \\ -\omega_2 & \omega_1 & 0 \end{bmatrix} \begin{bmatrix} J_{11} & J_{12} & J_{13} \\ J_{21} & J_{22} & J_{23} \\ J_{31} & J_{32} & J_{33} \end{bmatrix} \begin{bmatrix} \omega_1 \\ \omega_2 \\ \omega_3 \end{bmatrix}$$

$$+ 3n^2 \begin{bmatrix} 0 & -C_{13} & C_{12} \\ C_{13} & 0 & -C_{11} \\ -C_{12} & C_{11} & 0 \end{bmatrix} \begin{bmatrix} J_{11} & J_{12} & J_{13} \\ J_{21} & J_{22} & J_{23} \\ J_{31} & J_{32} & J_{33} \end{bmatrix} \begin{bmatrix} C_{11} \\ C_{12} \\ C_{13} \end{bmatrix} + \begin{bmatrix} -u_1 + d_1 \\ -u_2 + d_2 \\ -u_3 + d_3 \end{bmatrix} \tag{7.112}$$

Na prática, essas equações são as mesmas da aula 9, onde se modelou a inserção de rodas de reação num satélite sujeito a gradiente gravitacional em órbita baixa e atitude relativa ao LVLH. A única diferença é que a derivada da quantidade de movimento angular do CMG foi englobada na variável "u" e suas equações individualizadas em 7.113. Também inseriu-se um "torque extra" d1, d2, d3 que representa um distúrbio.

where

$$C_{11} = -\sin\theta_2 \cos\theta_3$$
$$C_{12} = \cos\theta_1 \sin\theta_2 \sin\theta_3 + \sin\theta_1 \cos\theta_2$$
$$C_{13} = -\sin\theta_1 \sin\theta_2 \sin\theta_3 + \cos\theta_1 \cos\theta_2$$

Outra mudança diz respeito à sequência 231 de ângulos de Euler ao invés de 321, mas os autores continuam tratando os ângulos como rolamento, arfagem e guinada.

CMG momentum dynamics:

Em resumo, na prática, podemos usar as mesmas equações da aula 9 fazendo pequenas mudanças.

$$\begin{bmatrix} \dot{h}_1 \\ \dot{h}_2 \\ \dot{h}_3 \end{bmatrix} + \begin{bmatrix} 0 & -\omega_3 & \omega_2 \\ \omega_3 & 0 & -\omega_1 \\ -\omega_2 & \omega_1 & 0 \end{bmatrix} \begin{bmatrix} h_1 \\ h_2 \\ h_3 \end{bmatrix} = \begin{bmatrix} u_1 \\ u_2 \\ u_3 \end{bmatrix} \tag{7.113}$$

where subscripts 1, 2, 3 denote the roll, pitch, and yaw control axes whose origin is fixed at the mass center, with the roll axis in the flight direction, the pitch axis perpendicular to the orbit plane, and the yaw axis toward the Earth; (θ_1, θ_2, θ_3) are the roll, pitch, and yaw Euler angles of the body-fixed control axes with respect to the LVLH axes that rotate with the orbital angular velocity n; (ω_1, ω_2, ω_3) are the body-axis components of the absolute angular velocity of the vehicle; (J_{11}, J_{22}, J_{33}) are the moments of inertia; J_{ij} ($i \neq j$) are the products of inertia; (h_1, h_2, h_3) are the body-axis components of the CMG momentum; (u_1, u_2, u_3) are the body-axis components of the control torque caused by CMG momentum change; (d_1, d_2, d_3) are the body-axis components of the external disturbance torque; and n is the orbital rate.

Without loss of generality, we consider in this section a large space vehicle shown in Fig. 7.4 with the following inertia matrix:

$$\begin{bmatrix} J_{11} & J_{12} & J_{13} \\ J_{21} & J_{22} & J_{23} \\ J_{31} & J_{32} & J_{33} \end{bmatrix} = \begin{bmatrix} 50.28 & -0.39 & 0.16 \\ -0.39 & 10.80 & 0.16 \\ 0.16 & 0.16 & 58.57 \end{bmatrix} \times 10^6 \text{ slug-ft}^2$$

The uncontrolled vehicle is in an unstable equilibrium when $\theta_1 = \theta_2 = \theta_3 = 0$. The external disturbance torque mainly consists of aerodynamic drag torque that can be modeled as bias plus cyclic terms in the body-fixed control axes; i.e., d_i in foot-pound are modeled as

Torque de distúrbio específico da ISS, não pode ser usado em outros satélites.

$$\begin{aligned} d_1 &= 1 + \sin(nt) + 0.5\sin(2nt) \\ d_2 &= 4 + 2\sin(nt) + 0.5\sin(2nt) \\ d_3 &= 1 + \sin(nt) + 0.5\sin(2nt) \end{aligned}$$

where $n = 0.0011$ rad/s, and magnitudes and phases are unknown for control design. The cyclic component at orbital rate is due to the effect of the Earth's diurnal bulge, whereas the cyclic torque at twice the orbital rate is caused by the rotating solar panels.

For small attitude deviations from LVLH orientation, the linearized equations of motion can be obtained as follows.

Attitude kinematics:

$$\dot{\theta}_1 - n\theta_3 = \omega_1 \tag{7.114a}$$

$$\dot{\theta}_2 - n = \omega_2 \tag{7.114b}$$

$$\dot{\theta}_3 + n\theta_1 = \omega_3 \tag{7.114c}$$

Rigid-body dynamics:

$$\begin{bmatrix} J_{11} & J_{12} & J_{13} \\ J_{21} & J_{22} & J_{23} \\ J_{31} & J_{32} & J_{33} \end{bmatrix} \begin{bmatrix} \dot{\omega}_1 \\ \dot{\omega}_2 \\ \dot{\omega}_3 \end{bmatrix} = n \begin{bmatrix} J_{31} & 2J_{32} & J_{33} - J_{22} \\ -J_{32} & 0 & J_{12} \\ J_{22} - J_{11} & -2J_{12} & -J_{13} \end{bmatrix} \begin{bmatrix} \omega_1 \\ \omega_2 \\ \omega_3 \end{bmatrix} + 3n^2 \begin{bmatrix} J_{33} - J_{22} & J_{21} & 0 \\ J_{12} & J_{33} - J_{11} & 0 \\ -J_{13} & -J_{23} & 0 \end{bmatrix} \begin{bmatrix} \theta_1 \\ \theta_2 \\ \theta_3 \end{bmatrix} + n^2 \begin{bmatrix} -2J_{23} \\ 3J_{13} \\ -J_{12} \end{bmatrix} + \begin{bmatrix} -u_1 + d_1 \\ -u_2 + d_2 \\ -u_3 + d_3 \end{bmatrix} \tag{7.115}$$

CMG momentum dynamics:

$$\dot{h}_1 - nh_3 = u_1 \tag{7.116a}$$

$$\dot{h}_2 = u_2 \tag{7.116b}$$

$$\dot{h}_3 + nh_1 = u_3 \tag{7.116c}$$

Combining Eqs. (7.114) and (7.115), we obtain the linearized equations of motion as

$$\begin{bmatrix} J_{11} & J_{12} & J_{13} \\ J_{21} & J_{22} & J_{23} \\ J_{31} & J_{32} & J_{33} \end{bmatrix} \begin{bmatrix} \ddot{\theta}_1 \\ \ddot{\theta}_2 \\ \ddot{\theta}_3 \end{bmatrix} = n \begin{bmatrix} 0 & 2J_{32} & J_{11} - J_{22} + J_{33} \\ -2J_{32} & 0 & 2J_{12} \\ -J_{11} + J_{22} - J_{33} & -2J_{12} & 0 \end{bmatrix} \begin{bmatrix} \dot{\theta}_1 \\ \dot{\theta}_2 \\ \dot{\theta}_3 \end{bmatrix} + n^2 \begin{bmatrix} 4(J_{33} - J_{22}) & 3J_{21} & -J_{31} \\ 4J_{12} & 3(J_{33} - J_{11}) & J_{32} \\ -4J_{13} & -3J_{23} & J_{11} - J_{22} \end{bmatrix} \begin{bmatrix} \theta_1 \\ \theta_2 \\ \theta_3 \end{bmatrix} + n^2 \begin{bmatrix} -4J_{23} \\ 3J_{13} \\ J_{12} \end{bmatrix} + \begin{bmatrix} -u_1 + d_1 \\ -u_2 + d_2 \\ -u_3 + d_3 \end{bmatrix} \tag{7.117}$$

Note that the products of inertia cause three-axis coupling as well as a bias torque in each axis. Fortunately, most practical situations of interest with small products of inertia permit further simplification in such a way that pitch motion is uncoupled from roll/yaw motion. Otherwise, Eq. (7.117) should be used for three-axis coupled stability analysis and control design.

For most practical cases in which the control axes are nearly aligned with the principal axes, i.e., $J_1 = J_{11}$, $J_2 = J_{22}$, and $J_3 = J_{33}$, and attitude deviations from the desired LVLH orientation are small, we have the following set of linearized equations of motion for control design:

$$J_1 \dot{\omega}_1 + n(J_2 - J_3)\omega_3 + 3n^2(J_2 - J_3)\theta_1 = -u_1 + d_1 \tag{7.118a}$$

$$J_2 \dot{\omega}_2 + 3n^2(J_1 - J_3)\theta_2 = -u_2 + d_2 \tag{7.118b}$$

$$J_3 \dot{\omega}_3 - n(J_2 - J_1)\omega_1 = -u_3 + d_3 \tag{7.118c}$$

$$\dot{\theta}_1 - n\theta_3 = \omega_1 \tag{7.118d}$$

$$\dot{\theta}_2 - n = \omega_2 \tag{7.118e}$$

$$\dot{\theta}_3 + n\theta_1 = \omega_3 \tag{7.118f}$$

$$\dot{h}_1 - nh_3 = u_1 \tag{7.118g}$$

$$\dot{h}_2 = u_2 \tag{7.118h}$$

$$\dot{h}_3 + nh_1 = u_3 \tag{7.118i}$$

A set of linearized equations of motion in terms of θ_i and h_i can also be obtained as

$$J_1 \ddot{\theta}_1 + 4n^2(J_2 - J_3)\theta_1 - n(J_1 - J_2 + J_3)\dot{\theta}_3 = -u_1 + d_1 \tag{7.119a}$$

$$J_2 \ddot{\theta}_2 + 3n^2(J_1 - J_3)\theta_2 = -u_2 + d_2 \tag{7.119b}$$

As equações 7.119a, 7.119b e 7.119c são as mesmas de dinâmica linearizada com torque de gradiente gravitacional da aula 7, com a adição de torques -u1+d1, -u2+d2, -u3+d3.

As equações 7.119d, 7.119e e 7.119f resultam na mesma dinâmica linearizada com torque de gradiente gravitacional e rodas de reação da aula 9, basta substituir u1, u2 e u3 nas equações 7.119a, 7.119b e 7.119c. Então, qual a diferença entre rodas de reação e CMG? A lógica interna de acionamento do CMG, que é altamente não linear devido aos guimbais de 2 graus de liberdade. Como isso foi idealizado no modelo, elaborando um equacionamento de alto nível onde os torques u1, u2 e u3 são demandas atendidas com perfeição, os modelos ficam iguais, onde ambos dispositivos são simplesmente ações de controle por meio da variação da qma, com armazenamento interno de qma, que precisa ser dessaturada.

$$J_3\ddot{\theta}_3 + n^2(J_2 - J_1)\theta_3 + n(J_1 - J_2 + J_3)\dot{\theta}_1 = -u_3 + d_3 \tag{7.119c}$$

$$\dot{h}_1 - nh_3 = u_1 \tag{7.119d}$$

$$\dot{h}_2 = u_2 \tag{7.119e}$$

$$\dot{h}_3 + nh_1 = u_3 \tag{7.119f}$$

Certain assembly configurations of the large space vehicle shown in Fig. 7.4 may need a large torque equilibrium attitude (TEA) in the pitch axis because of the small gravity-gradient torque available in the pitch axis. In such cases, Eqs. (7.111) and (7.112) with small roll/yaw attitude errors and small products of inertia become

Equações obtidas quando não é possível fazer o ângulo de arfagem pequeno, não sendo corretas as aproximações sen(theta2)=theta2 e cos(theta2)=1. Assim, tais termos permanecem nas equações.

$$J_1\ddot{\theta}_1 + \left(1 + 3\cos^2\theta_2\right)n^2(J_2 - J_3)\theta_1 - n(J_1 - J_2 + J_3)\dot{\theta}_3 + 3(J_2 - J_3)n^2(\sin\theta_2\cos\theta_2)\theta_3 = -u_1 + d_1 \tag{7.120a}$$

$$J_2\ddot{\theta}_2 + 3n^2(J_1 - J_3)\sin\theta_2\cos\theta_2 = -u_2 + d_2 \tag{7.120b}$$

$$J_3\ddot{\theta}_3 + \left(1 + 3\sin^2\theta_2\right)n^2(J_2 - J_1)\theta_3 + n(J_1 - J_2 + J_3)\dot{\theta}_1 + 3(J_2 - J_1)n^2(\sin\theta_2\cos\theta_2)\theta_1 = -u_3 + d_3 \tag{7.120c}$$

It is evident from this set of equations that roll/yaw motion is affected by pitch motion. If pitch attitude is held constant with respect to the pitch TEA, the roll/yaw equations can be considered time invariant. These equations are also useful for roll/yaw controller design for the large space vehicle shown in Fig. 7.4 with a large pitch TEA.

O projeto de controle é feito para as equações lineares simplificadas, mas a simulação para teste precisa ser realizada com o modelo não linear completo.

7.4.3 Pitch Control Design

Equation (7.119b), which is uncoupled from the roll/yaw equations, is used as the basis for pitch control analysis and design. A block diagram of the pitch-axis momentum/attitude control system is shown in Fig. 7.5. First we consider a control design that does not include the indicated cyclic- or periodic-disturbance rejection filter $R_2(s)$ followed by a control design that includes the filter.

7.4.3.1 Pitch Control without Periodic-disturbance Rejection The pitch-axis controller consists of a single control input u_2 and four states: θ_2, $\dot{\theta}_2$, h_2, and $\int h_2$. The pitch control logic is then given by

Variáveis de estado:

$\theta_2, \dot{\theta}_2, h_2, \int h_2$

$$u_2 = K_{2P}\theta_2 + K_{2D}\dot{\theta}_2 + K_{2H}\,h_2 + K_{2I}\int h_2 \tag{7.121}$$

where the pitch-axis CMG momentum and its integral are included to prevent momentum buildup.

Various methods may be employed for the selection of the four gains of Eq. (7.121). A pole placement technique may be used to place the closed-loop eigenvalues at any desired location. The practical problem with this approach is that it is not always clear where to place the eigenvalues for satisfactory performance and robustness.

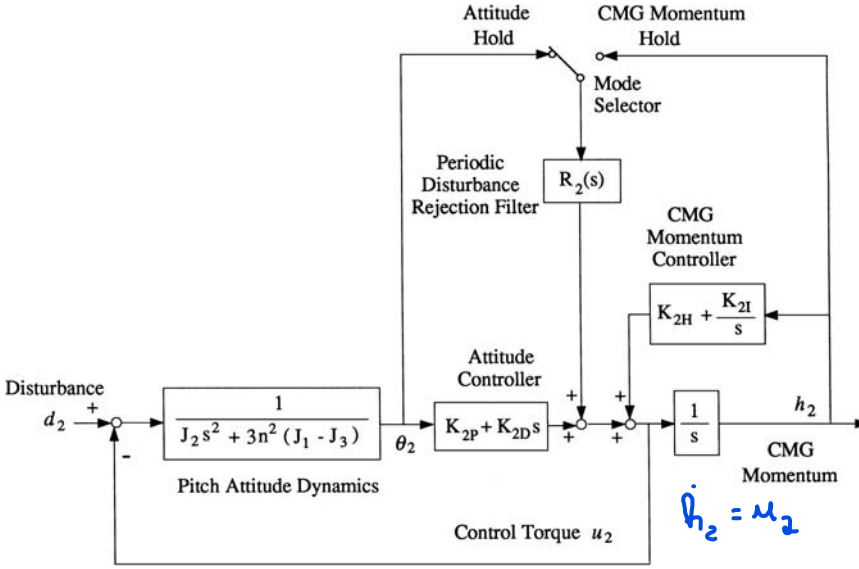

Fig. 7.5 Pitch-axis attitude and CMG momentum control system.

Pitch control design by iterative successive loop closures is possible, but quite tedious. The pitch controller can also be synthesized using an equivalent compensator. This approach provides physical insight into the proper tradeoff between the attitude control and the momentum management. Combining Eqs. (7.118h) and (7.121) to eliminate h_2 gives an equivalent compensator of the form

Compensador resultante das malhas da figura 7.5

$$u_2 = \frac{s^2(K_{2P} + sK_{2D})}{s^2 - K_{2H}s - K_{2I}}\,\theta_2 \tag{7.122}$$

The integrated momentum/attitude controller can be interpreted as a second-order compensator with four parameters. The momentum controller consists of double zeros at the origin and complex poles. The attitude controller consists of one zero on the real axis, which is a conventional proportional-derivative controller. An unstable compensator is needed to stabilize the unstable system. It can be easily shown that $h_2(s)/d_2(s)$ of the closed-loop system has a zero at $s = 0$. Thus, $h_2(t)$ has zero steady-state value for a constant disturbance.

LQR synthesis of the pitch control with full-state feedback can be quickly accomplished using a computer code. The LQR technique makes use of a quadratic performance index to synthesize state-feedback gains that minimize the index, as was discussed in Chapter 2. It is especially useful for multivariable systems; all loops are closed simultaneously instead of successively as in classical frequency-domain methods. The problem with this approach, however, is that the proper selection of the weighting matrices is not obvious. It is not always possible to predict the effects of given weighting matrices on the closed-loop behavior.

A practical approach to the pitch-axis controller design would be to find the control gains and closed-loop poles that result from a wide range of weighting matrices, and to simulate the corresponding closed-loop system. The gain matrix that produces the closed-loop responses satisfying the various requirements would become the final selection.

7.4.3.2 Pitch Control with Periodic-disturbance Rejection Depending on the circumstances, either pitch attitude or CMG momentum oscillation, caused by the aerodynamic disturbance torque, may be undesirable. In such cases, a periodic-disturbance rejection filter can be employed as was illustrated in Fig. 7.5.

The periodic-disturbance rejection filter is represented as

$$R_2(s) = \frac{N_2(s)}{[s^2 + n^2][s^2 + (2n)^2]} \tag{7.123}$$

The filter poles will appear in the numerator of the closed-loop transfer function $\theta_2(s)/d_2(s)$ or $h_2(s)/d_2(s)$, depending on mode selection. This results in a disturbance rejection at frequencies of n and $2n$ for either θ_2 or h_2. The filter numerator $N_2(s)$ should be properly designed to stabilize the overall control system.

The disturbance rejection filter for θ_2 can also be represented as

Ficou estranha essa equação de estado do filtro composta de duas equações de estado com a mesma entrada.

$$\ddot{\alpha}_2 + (n)^2\alpha_2 = \theta_2 \tag{7.124a}$$

$$\ddot{\beta}_2 + (2n)^2\beta_2 = \theta_2 \tag{7.124b}$$

where initial conditions for α_2, β_2, $\dot{\alpha}_2$, and $\dot{\beta}_2$ can be arbitrarily selected (usually zero initial conditions). These filter equations are integrated in the onboard computer. Each filter equation passes the filter states that carry undesired frequency components of θ_2. For example, α_2 and $\dot{\alpha}_2$ carry the frequency component of θ_2 at the orbital frequency n. The undesired component is rejected by feeding back the filter states.

The pitch control logic, with additional disturbance rejection filter states, can then be expressed as

$$u_2 = K_{2P}\theta_2 + K_{2D}\dot{\theta}_2 + K_{2H}h_2 + K_{2I}\int h_2 + K_{2\alpha}\alpha_2 + K_{2\dot{\alpha}}\dot{\alpha}_2 + K_{2\beta}\beta_2 + K_{2\dot{\beta}}\dot{\beta}_2 \tag{7.125}$$

Os ganhos de realimentação do filtro são provenientes do numerador N2(s)?

It is also possible to provide periodic-disturbance rejection for the pitch-axis CMG momentum. For this case, θ_2 of Eqs. (7.124) is replaced by h_2. Proper gains of Eq. (7.125) are then selected. Depending on the specific mission requirements, either pitch attitude or CMG momentum can be held constant by employing the pitch controller illustrated in Fig. 7.5.

Problems

7.18 Consider the pitch-axis control design of the large space vehicle shown in Fig. 7.4.

Table 7.1 Closed-loop eigenvalues in units of orbital rate, n = 0.0011 rad/s

	Momentum/attitude		Disturbance filter	
Pitch	$-1.0,\ -1.5$	$-1.5 \pm 1.5j$	$-0.3 \pm 1.0j$	$-0.3 \pm 2.0j$
Roll/yaw	$-0.23,\ -0.68$	$-0.66 \pm 1.51j$	$-0.23 \pm 0.92j$	$-0.20 \pm 2.02j$
	$-1.02 \pm 0.29j$	$-1.50 \pm 0.84j$	$-0.26 \pm 1.04j$	$-0.62 \pm 2.29j$

(a) Given the desired closed-loop eigenvalues $-1.5n$, $-1.0n$, and $(-1.5 \pm 1.5j)n$, determine a set of four gains of the pitch-axis control logic (7.121).

Note: If an LQR code, instead of the pole-placement technique, is to be employed, then determine a set of four gains for a control bandwidth of approximately $1.5n$.

(b) Obtain the closed-loop, frequency-response magnitude plots of

$$\frac{\theta_2(s)}{d_2(s)} \quad \text{and} \quad \frac{h_2(s)}{d_2(s)}$$

(c) Perform computer simulation of the closed-loop system (only pitch axis) subject to the aerodynamic disturbance d_2 and initial conditions $\theta_2(0) = 1$ deg and $\dot{\theta}_2(0) = 0.001$ deg/s.

Note: The periodic aerodynamic torque will cause the periodic responses of both pitch attitude and pitch-axis CMG momentum. The CMG momentum h_2 will be bounded with zero mean value, whereas θ_2 is oscillating with respect to a -7.5- deg pitch TEA.

7.19 Consider the periodic-disturbance rejection control design for the pitch-axis of the large space vehicle shown in Fig. 7.4.

(a) Determine a set of eight gains of the pitch-axis control logic (7.125) to achieve the desired closed-loop eigenvalues listed in Table 7.1.

Note: If an LQR code, instead of the pole-placement technique, is to be employed, then design a controller for a control bandwidth of approximately $1.5n$ and for an asymptotic disturbance rejection within three orbits.

(b) Obtain the closed-loop, frequency-response magnitude plots of

$$\frac{\theta_2(s)}{d_2(s)} \quad \text{and} \quad \frac{h_2(s)}{d_2(s)}$$

(c) Perform computer simulation of the closed-loop system with the pitch-axis aerodynamic disturbance and initial conditions of $\theta_2(0) = 1$ deg and $\dot{\theta}_2(0) = 0.001$ deg/s.

Note: Because a disturbance rejection filter is used here for pitch attitude, an asymptotic disturbance rejection of a periodic disturbance of frequencies n and $2n$ will be achieved for the pitch attitude. The CMG momentum will be bounded with zero mean value, while the pitch attitude is held constant at a -7.5-deg pitch TEA after approximately two orbits.

7.4.4 Roll/Yaw Control Design

Similar to the pitch-axis control design, we consider here roll/yaw control design. Two cases are considered: the first without periodic-disturbance rejection filters and the second with the filters.

7.4.4.1 Roll/yaw Control without Periodic-disturbance Rejection The first case of roll/yaw control design consists of two inputs u_1 and u_3, and eight states, including two integral states for the CMG momentum. The eight states are the roll-axis θ_1, ω_1, h_1, and $\int h_1$; and the yaw-axis θ_3, ω_3, h_3, and $\int h_3$. Note that body rates ω_1 and ω_3, instead of $\dot{\theta}_1$ and $\dot{\theta}_3$, are used as state variables.

The roll/yaw full-state feedback controller can be designed, iteratively, using the linear quadratic regulator (LQR) or pole-placement techniques. The multi-input characteristics of the roll/yaw axes, however, provide for the calculation of various gain matrices that yield the same closed-loop eigenvalues. Although the gain matrix can be completely specified by assigning not only the closed-loop eigenvalues but also an allowable set of closed-loop eigenvectors, the conventional LQR technique can be employed to find a closed-loop system satisfying various requirements.

7.4.4.2 Roll/yaw Control with Periodic-disturbance Rejection For the reduction of the steady-state oscillation of roll/yaw attitude and CMG momentum, periodic-disturbance rejection filtering for a multivariable system is described here.

Combining Eqs. (7.119a), (7.119c), (7.119d), and (7.119f), we obtain the transfer function matrix description of the coupled roll/yaw dynamics as

$$\begin{bmatrix} \theta_1(s) \\ \theta_3(s) \end{bmatrix} = \frac{1}{\Delta} \begin{bmatrix} G_{11} & G_{13} \\ G_{31} & G_{33} \end{bmatrix} \begin{bmatrix} u_1(s) - d_1(s) \\ u_3(s) - d_3(s) \end{bmatrix} \tag{7.126}$$

$$\begin{bmatrix} h_1(s) \\ h_3(s) \end{bmatrix} = \frac{1}{s^2 + n^2} \begin{bmatrix} s, & n \\ -n, & s \end{bmatrix} \begin{bmatrix} u_1(s) \\ u_3(s) \end{bmatrix} \tag{7.127}$$

where

$$\Delta = J_1 J_3 (s^2 + n^2)\left[s^4 + (1 + 3k_1 + k_1 k_3) n^2 s^2 + 4k_1 k_3 n^4\right]$$

$$G_{11} = -\left[J_3 s^2 + (J_2 - J_1) n^2\right](s^2 + n^2)$$

$$G_{13} = -(J_1 - J_2 + J_3) ns(s^2 + n^2) = -G_{31}$$

$$G_{33} = -\left[J_1 s^2 + 4(J_2 - J_3) n^2\right](s^2 + n^2)$$

$$k_1 = (J_2 - J_3)/J_1 \qquad \text{and} \qquad k_3 = (J_2 - J_1)/J_3$$

It is apparent that $\pm nj$ are transmission zeros of Eq. (7.126). In other words, a periodic disturbance at orbital rate cannot be rejected for both roll and yaw attitude. In addition, it can be seen in Eq. (7.127) that resonance of CMG momentum can

happen for sinusoidal control inputs of frequency n. For this case, where the CMG momentum dynamics are described by Eq. (7.116), it is not evident why a periodic disturbance at orbital rate can be rejected for the yaw attitude and not for the roll attitude.

To investigate such inherent characteristics of the coupled roll/yaw dynamics, the following CMG momentum dynamics, with a proper modification of the equations of motion of the vehicle, are considered:

$$\dot{h}_1 = u_1 \tag{7.128a}$$

$$\dot{h}_3 = u_3 \tag{7.128b}$$

For this case, the following transfer function matrix description can be obtained as:

$$\begin{bmatrix}\theta_1(s)\\ \theta_3(s)\end{bmatrix} = \frac{1}{\Delta}\begin{bmatrix}G_{11} & G_{13}\\ G_{31} & G_{33}\end{bmatrix}\begin{bmatrix}u_1(s)\\ u_3(s)\end{bmatrix}$$

$$+\frac{s^2}{\Delta}\begin{bmatrix}J_3s^2+(J_2-J_1)n^2 & (J_1-J_2+J_3)ns\\ -(J_1-J_2+J_3)ns & J_1s^2+4(J_2-J_3)n^2\end{bmatrix}\begin{bmatrix}d_1(s)\\ d_3(s)\end{bmatrix} \tag{7.129}$$

$$\begin{bmatrix}h_1(s)\\ h_3(s)\end{bmatrix} = \frac{1}{s}\begin{bmatrix}1 & 0\\ 0 & 1\end{bmatrix}\begin{bmatrix}u_1(s)\\ u_3(s)\end{bmatrix} \tag{7.130}$$

where

$$\Delta = J_1J_3s^2\left[s^4+(1+3k_1+k_1k_3)n^2s^2+4k_1k_3n^4\right]$$

$$G_{11} = -J_3s^2(s^2+n^2)$$

$$G_{13} = (J_2-J_1)ns(s^2+n^2)$$

$$G_{31} = (J_3-J_2)ns[s^2+(2n)^2]$$

$$G_{33} = -s^2\left[J_1s^2+(J_1+3J_2-3J_3)n^2\right]$$

$$k_1 = (J_2-J_3)/J_1 \qquad \text{and} \qquad k_3 = (J_2-J_1)/J_3$$

It can be shown that $\pm nj$ are transmission zeros of the transfer function matrix from (u_1, u_3) to (θ_1, θ_3). The zero at $s = \pm nj$ appears in both the $\theta_1(s)/u_1(s)$ and $\theta_1(s)/u_3(s)$ transfer functions, but not in yaw attitude channels. Therefore, a periodic-disturbance rejection at the orbital rate is not possible for roll attitude, whereas it is possible for yaw attitude. Furthermore, it can be shown that $\pm nj$ are not transmission zeros of the transfer function matrix from (u_1, u_3) to (h_1, θ_3). Consequently, a periodic-disturbance rejection for the roll-axis CMG momentum and yaw attitude can be achieved by employing roll/yaw periodic-disturbance

rejection filters of the form

$$\ddot{\alpha}_1 + (n)^2\alpha_1 = h_1 \tag{7.131a}$$

$$\ddot{\beta}_1 + (2n)^2\beta_1 = h_1 \tag{7.131b}$$

$$\ddot{\alpha}_3 + (n)^2\alpha_3 = \theta_3 \tag{7.131c}$$

$$\ddot{\beta}_3 + (2n)^2\beta_3 = \theta_3 \tag{7.131d}$$

Problems

7.20 Consider the large space vehicle shown in Fig. 7.4, which is unstable in roll/yaw and has open-loop poles of $(\pm 1.05 \pm 0.7j)n$, $\pm nj$. The roll/yaw control logic is described by

$$\begin{bmatrix} u_1 \\ u_3 \end{bmatrix} = \begin{bmatrix} \mathbf{K}_{11} & \mathbf{K}_{13} \\ \mathbf{K}_{31} & \mathbf{K}_{33} \end{bmatrix} \begin{bmatrix} \mathbf{x}_1 \\ \mathbf{x}_3 \end{bmatrix}$$

where $\mathbf{K}_{ij}$ are 1×4 gain matrices and

$$\mathbf{x}_1 = \begin{bmatrix} \theta_1 & \omega_1 & h_1 & \int h_1 \end{bmatrix}^T$$

$$\mathbf{x}_3 = \begin{bmatrix} \theta_3 & \omega_3 & h_3 & \int h_3 \end{bmatrix}^T$$

(a) Determine a 2×8 gain matrix of the roll/yaw control logic for the following desired closed-loop poles: $(-1.05 \pm 0.68j)n$, $(-1.04 \pm 0.72j)n$, $(-1.42 \pm 1.38j)n$, and $(-1.42 \pm 1.38j)n$.

Note: If an LQR code, instead of the eigenstructure assignment technique, is to be employed, then design a controller for a control bandwidth of approximately $1.5n$.

(b) Obtain the closed-loop, frequency-response magnitude plots of

$$\frac{\theta_1(s)}{d_1(s)}, \qquad \frac{h_1(s)}{d_1(s)}, \qquad \frac{\theta_3(s)}{d_3(s)}, \qquad \text{and} \qquad \frac{h_3(s)}{d_3(s)}$$

(c) Perform computer simulation of the closed-loop system subject to roll/yaw aerodynamic disturbances and initial conditions $\theta_1(0) = \theta_3(0) = 1$ deg and $\omega_1(0) = \omega_3(0) = 0.001$ deg/s.

7.21 Consider the large space vehicle of the preceding problem but with the roll/yaw control logic, employing the periodic-disturbance filters described by Eqs. (7.131), of the form

$$\begin{bmatrix} u_1 \\ u_3 \end{bmatrix} = \begin{bmatrix} \mathbf{K}_{11} & \mathbf{K}_{13} \\ \mathbf{K}_{31} & \mathbf{K}_{33} \end{bmatrix} \begin{bmatrix} \mathbf{x}_1 \\ \mathbf{x}_3 \end{bmatrix}$$

where $\mathbf{K}_{ij}$ are 1×8 gain matrices and

$$\mathbf{x}_1 = \begin{bmatrix} \theta_1 & \omega_1 & h_1 & \int h_1 & \alpha_1 & \dot{\alpha}_1 & \beta_1 & \dot{\beta}_1 \end{bmatrix}^T$$

$$\mathbf{x}_3 = \begin{bmatrix} \theta_3 & \omega_3 & h_3 & \int h_3 & \alpha_3 & \dot{\alpha}_3 & \beta_3 & \dot{\beta}_3 \end{bmatrix}^T$$

(a) Determine a 2×16 gain matrix for the desired closed-loop eigenvalues as listed in Table 7.1.

Note: If an LQR code, instead of the eigenstructure assignment technique, is to be employed, then design a controller for a control bandwidth of approximately $1.5n$ and for an asymptotic disturbance rejection within three orbits.

(b) Obtain the closed-loop, frequency-response magnitude plots of

$$\frac{\theta_1(s)}{d_1(s)}, \qquad \frac{h_1(s)}{d_1(s)}, \qquad \frac{\theta_3(s)}{d_3(s)}, \qquad \text{and} \qquad \frac{h_3(s)}{d_3(s)}$$

(c) Show that $\pm nj$ are "blocking zeros" of the closed-loop transfer function matrix from (d_1, d_3) to (h_1, θ_3).

(d) Perform computer simulation of the closed-loop system subject to roll/yaw aerodynamic disturbances and initial conditions $\theta_1(0) = \theta_3(0) = 1$ deg and $\omega_1(0) = \omega_3(0) = 0.001$ deg/s.

Note: The roll-axis CMG momentum will approach zero steady-state value, whereas roll attitude oscillates at the orbital rate. The yaw attitude will approach a constant steady-state value, whereas the yaw-axis CMG momentum oscillates at the orbital rate. As a result, the overall attitude and CMG momentum oscillations are minimized.

7.22 Consider the large space vehicle of the preceding problems but with the roll/pitch/yaw control logic employing the periodic-disturbance rejection filters of the form

$$\begin{aligned}
\ddot{\alpha}_1 + (\,n\,)^2\alpha_1 &= h_1 \\
\ddot{\beta}_1 + (2n)^2\beta_1 &= h_1 \\
\ddot{\alpha}_2 + (\,n\,)^2\alpha_2 &= h_2 \\
\ddot{\beta}_2 + (2n)^2\beta_2 &= h_2 \\
\ddot{\alpha}_3 + (\,n\,)^2\alpha_3 &= h_3 \\
\ddot{\beta}_3 + (2n)^2\beta_3 &= h_3
\end{aligned}$$

(a) Design such a controller that will provide an asymptotic disturbance rejection for CMGs.

(b) Perform computer simulation of the closed-loop system subject to roll/pitch/yaw aerodynamic disturbances and initial conditions $\theta_1(0) = \theta_2(0) = \theta_3(0) = 1$ deg, $\omega_1(0) = \omega_3(0) = 0.001$ deg/s, and $\dot{\theta}_2(0) = 0.001$ deg/s.

7.4.5 Robust Control Design

We now consider a robust control design problem of the large space vehicle shown in Fig. 7.4. The objective is to design a constant-gain controller that may yield the largest stable hypercube in uncertain parameter space, subject to the nominal performance requirements. However, the robust control design does not